

1 **Mechanical Formation of Micro- and Nano-Plastic Materials for Environmental Studies**  
2 **in Agricultural Ecosystems**

3 A.F. Astner<sup>1</sup>, D.G. Hayes<sup>1</sup>, H. O'Neill<sup>2</sup>, B.R. Evans<sup>2</sup>, S. V. Pingali<sup>2</sup>, V.S. Urban<sup>2</sup>, T.M Young<sup>3</sup>

4

5 **ABSTRACT:**

6 Release of microplastics (MPs) and nanoplastics (NPs) into agricultural fields is of great concern  
7 due to their reported ecotoxicity to organisms that provide beneficial service to the soil such as  
8 earthworms, and the potential ability of MPs and NPs to enter the food chain. Most fundamental  
9 studies of the life cycle, fate and transport of plastic particulates in the terrestrial environment  
10 employ idealized MP materials as models, such as monodisperse polystyrene spheres. In contrast,  
11 plastics that reside in agricultural soils consist of polydisperse fragments resulting from degraded  
12 polyethylene (PE)-based films used as high-tunnel covers and mulch films and other agricultural  
13 plastic materials employed in specialty crop production. There exists a need for more  
14 representative materials in fundamental studies of the fate, transport, and ecotoxicity of MPs and  
15 NPs in soil ecosystems. The objective of this study was therefore to develop a procedure that  
16 produces MPs and NPs from agricultural plastics (a mulch film prepared biodegradable polymer  
17 polybutyrate adipate-co-terephthalate (PBAT) and low-density PE [LDPE]), and to characterize  
18 the resultant materials. Soaking of PBAT films into liquid nitrogen / water mixtures under  
19 cryogenic conditions promoted embrittlement, similar to what occurs through environmental  
20 weathering. LDPE and cryogenically-treated PBAT underwent mechanical milling followed by  
21 sieve fractionation into MP fractions of 840  $\mu\text{m}$ , 250  $\mu\text{m}$ , 106  $\mu\text{m}$ , and 45  $\mu\text{m}$ , with recovery of  
22 the latter two fractions being 2% and 1%, respectively, for each polymeric material. The 106  $\mu\text{m}$   
23 fraction was subjected to wet grinding to produce NPs of average particle size 366.0 nm and

24 389.4 nm for PBAT and LDPE, respectively. A two-parameter Weibull model described the  
25 MPs' particle size distributions, while NPs possessed bimodal distributions of the two-parameter  
26 Weibull model. Size reduction did not produce any changes in the chemical properties of the  
27 plastics, except for slight depolymerization and an increase of crystallinity resulting from  
28 cryogenic treatment. This study suggests that MPs form from cutting and high-impact  
29 mechanical degradation as would occur during the tillage into soil, and that NPs form from the  
30 MP fragments in regions of relative weakness that possess lower molecular weight polymers and  
31 crystallinity.

32

33 **KEYWORDS:** agricultural soils, low-density polyethylene (LDPE), microplastics,  
34 nanoplastics, polybutylene adipate-co-terephthalate (PBAT), terrestrial ecosystems

35

36 **FUNDING SOURCES:** University of Tennessee (Institute for a Secure and Sustainable  
37 Environment), US Department of Agriculture (grant numbers and further information given in  
38 the *Acknowledgements* section)

39

40 **ABBREVIATIONS:**

41 **AIC:** Akaike's information criterion (used to assess the quality of the Weibull model to the  
42 fitting of particle size distribution data)

43 **BIC:** Bayesian information criterion (used to assess the quality of the Weibull model to the  
44 fitting of particle size distribution data)

45 **DSC:** differential scanning calorimetry

46 **DLS:** dynamic light scattering

- 47  **$d_p$** : average particle size (diameter)
- 48 **DTG**: differential thermogram (DSC analysis)
- 49 **FTIR**: Fourier transform infrared spectroscopy
- 50 **GPC**: gel permeation chromatography
- 51 **LDPE**: low-density polyethylene
- 52  **$M_n$** : number-averaged molecular weight
- 53 **MP**: microplastic
- 54  **$M_w$** : weight-averaged molecular weight
- 55 **NP**: nanoplastic
- 56 **PBAT**: polybutylene adipate-co-terephthalate
- 57 **PDI**: polydispersity index (for molecular weight)
- 58 **TGA**: thermogravimetric analysis
- 59  **$X_c$** : mole fraction of crystalline morphology for PBAT, **Eq. S1**
- 60  **$\alpha$** : scale parameter for the two-parameter Weibull model, **Eq. 1**
- 61  **$\beta$** : shape parameter for the two-parameter Weibull model, **Eq. 1**
- 62
- 63
- 64
- 65
- 66
- 67
- 68
- 69

## 70 1. INTRODUCTION

71 The rapid increase of global plastic production (322 million tons; 5% annual growth),  
72 combined with minimal recycling and improper disposal have led to increased release of post-  
73 consumer plastics into the environment (e.g., 250 million metric tonnes of plastic in the oceans  
74 projected for 2025, equivalent to 5.25 trillion plastic particles) (Alimi et al., 2018; Jambeck et  
75 al., 2015; Mattsson et al., 2015; Wright and Kelly, 2017). The plastic materials, originally macro-  
76 or meso-plastics (average particle size [diameter], or  $d_p$ , of > 25 mm and 5-25 mm, respectively)  
77 undergo size reduction due to shear, chemical and biochemical reactions, resulting in  
78 defragmentation into micro- and nanoplastics (MPs and NPs, respectively) to produce  $d_p$  of 0.1-  
79 5000  $\mu\text{m}$  and 1-1000 nm, respectively (Alimi et al., 2018; Gigault et al., 2018; Hartmann et al.,  
80 2019). (A thorough discussion on the defining size range for NPs is given in (Gigault et al.,  
81 2018).) Plastic litter accumulates in various environments, including marine (Alimi et al., 2018)  
82 and terrestrial (Horton et al., 2017; Nizzetto et al., 2016; Scheurer and Bigalke, 2018) habitats.  
83 The small plastic fragments exhibit major environmental health concerns impacting marine and  
84 terrestrial environment, either directly or as carriers of pesticides, plasticizers, or other  
85 potentially harmful agents (Bouwmeester et al., 2015; Koelmans et al., 2013). Most studies of  
86 ecotoxicity formation and behavior of MPs and NPs have been reported for marine environments,  
87 showing potential harm to microorganisms (Eckert et al., 2018; McCormick et al., 2014)  
88 (including the microbiome of macroorganisms (Lu et al., 2018; Oberbeckmann et al., 2018; Zhu  
89 et al., 2018)), fish, and other macroorganisms (Alimi et al., 2018; Bouwmeester et al., 2015;  
90 Horton et al., 2017; Mattsson et al., 2015). Recent studies have detected MPs in humans and  
91 other mammals, resulting from accumulation in the food chain (Bouwmeester et al., 2015; Efsa

92 Panel on Contaminants in the Food Chain, 2016; Lu et al., 2018; Schwabl et al., 2018; Wright  
93 and Kelly, 2017).

94 In contrast, terrestrial MPs have been investigated only to a minimal extent, despite their  
95 presence at higher amounts compared to marine plastics (Alimi et al., 2018; Bläsing and  
96 Amelung, 2018; Horton et al., 2017; Nizzetto et al., 2016), and the detection of terrestrial NPs  
97 have not been reported in the literature to the best of our knowledge (although they are likely to  
98 occur (Ng et al., 2018)). Recent studies reported that MPs harm soil-dwelling organisms,  
99 earthworms and collembolans (hexapods) and microorganisms (Huerta Lwanga et al., 2017; Zhu  
100 et al., 2018).

101 The occurrence MPs and NPs on farmland is of particular concern, due to the potential  
102 harm to cropping and animal systems, which could lead to loss of agricultural productivity or  
103 accumulation of MPs and NPs in foods (Nizzetto et al., 2016). A major source of terrestrial  
104 plastic fragments are agricultural plastics, employed as coverings for high tunnels, silage film,  
105 drip tape, seed casings, plant trays and bags, and row covers (Hussain and Hamid, 2003;  
106 Scarascia-Mugnozza et al., 2011). The most extensive application of agricultural plastics is  
107 mulch film (Steinmetz et al., 2016), used in the production of vegetables and other specialty  
108 crops as covering on the soil to reduce weeds, control soil temperature, and prevent evaporative  
109 loss of soil moisture and erosion (Kasirajan and Ngouajio, 2012; Steinmetz et al., 2016). The  
110 global market for agricultural plastic films was 4 million tons (\$10.6 million) in 2016, and is  
111 projected to grow at a rate of 5.6% per year through 2030 (von Moos et al., 2012).

112 Polyethylene (PE) is the most commonly used polymer for mulch films and other  
113 agricultural plastics (Hussain and Hamid, 2003; Kasirajan and Ngouajio, 2012; Scarascia-  
114 Mugnozza et al., 2011). Opportunities for recycling of agricultural plastics are minimal, and

115 labor costs to retrieve plastic mulches after crop harvest are prohibitive to farmers (Kasirajan  
116 and Ngouajio, 2012; Miles et al., 2017). Often, agricultural plastics are stockpiled on farms for  
117 long duration, providing the opportunity for fragmentation. Furthermore, agricultural plastics  
118 become embrittled due to environmental weathering during their service life, with ultraviolet  
119 radiation being the most significant factor (Hayes et al., 2017). Therefore, hand-retrieval of  
120 plastics would likely not remove all plastic fragments, resulting in the dispersal of the plastics  
121 into soil and watersheds. **In addition,** PE is poorly biodegradable, allowing for its long-term  
122 retention in the environment (de Souza Machado et al., 2017; Kasirajan and Ngouajio, 2012;  
123 Nizzetto et al., 2016; Steinmetz et al., 2016). In summary, improper disposal of agricultural  
124 plastics, exacerbated by embrittlement via environmental weathering, leads to the dispersal of  
125 the plastic fragments into agricultural soils.

126 To address the problems associated with PE mulch, biodegradable plastic mulches  
127 (BDMs) have been developed. These films, containing biodegradable polymeric blends that  
128 mimic the desirable mechanical properties of PE (e.g., high tensile stress and elongation, as  
129 possessed by blends enriched in polybutyrate, i.e., polybutylene adipate-co terephthalate  
130 [PBAT]), are designed to be plowed into the field after the harvesting of the crop, where they  
131 should be fully biodegraded by soil-borne microorganisms into CO<sub>2</sub> and water within a ~2-year  
132 period (Hayes et al., 2019; Kasirajan and Ngouajio, 2012; Steinmetz et al., 2016). Therefore,  
133 since the biodegradation rate in soil is slow, MPs and NPs may reside in the soil for several  
134 months, and we have detected μPs from BDMs in soil at 20-40 kg/ha (M. English and S.M.  
135 Schaeffer, personal communication).

136 Fundamental studies are required to understand the behavior, fate and transport of MPs  
137 and NPs in terrestrial environments, as well as for ecotoxicity and adsorption of toxicants such

138 as pesticides and plasticizers. Such studies should employ representative MP and NP models.  
139 Yet, most investigations have employed overly simplified or non-representative MP and NP  
140 materials such as monodisperse polystyrene spheres (Gigault et al., 2018). The absence of  
141 appropriate model MPs and NPs for terrestrial environments motivated the authors to prepare  
142 such models from agricultural plastics.

143 The methodology developed includes cryogenic soaking (to simulate embrittlement that  
144 typically occurs through environmental weathering (Hayes et al., 2017)), milling and sieve  
145 fractionation (to prepare different MP subpopulations and to simulate cutting and high-impact  
146 mechanical degradation, as would occur during tillage of plastics into the soil) followed by wet  
147 grinding (to prepare NPs) (Figure 1). Mild operating conditions of milling and wet grinding  
148 were chosen (e.g., minimization of residence time to reduce the significance of friction-induced  
149 heat generation) so that artifacts in the chemical nature of the polymers such as oxidation or  
150 cross-linking would not occur.

151 Exposure to cryogenic conditions followed by mechanical milling is well known to  
152 induce size reduction of polymeric materials (Dümichen et al., 2015; Goedecke et al., 2017;  
153 Jonna and Lyons, 2005; Poulouse et al., 2016; Robotti et al., 2016; Saba et al., 2015). A few recent  
154 studies have employed milling procedure to prepare model MPs from several different polymeric  
155 materials (e.g., polystyrene, polypropylene, PE and PBAT) for environmental research  
156 (Corradini et al., 2019; Eitzen et al., 2019; Guo et al., 2018; Kühn et al., 2018; Xu et al., 2018;  
157 Zuo et al., 2019). The majority of these studies produced MPs of size > 200 µm. (Guo et al.,  
158 2018) prepared MPs of PE, polypropylene, polystyrene and polyvinylchloride of size ~10-40  
159 µm, but used harsher mechanical grinding conditions that may have provided thermal  
160 degradation. (Eitzen et al., 2019) performed a similar low-temperature milling and sieving

161 approach to that employed herein, and obtained MP sizes of 5-100  $\mu\text{m}$ . However, the cited study  
162 employed polystyrene, an inherently brittle polymer that possesses lower impact strength than  
163 the polymeric materials employed herein that is not commonly employed in agriculture. The  
164 current study probes deeper than the previous studies in terms of the size distribution and  
165 physicochemical-related properties.

166 A unique aspect of this paper is the preparation of NPs from the MPs via wet grinding.  
167 Wet grinding is frequently employed to induce size reduction to the nanoscale (Elkharraz et al.,  
168 2003; Ravishankar et al., 2018; Schmidt et al., 2012; Schmidt et al., 2017; Watano et al., 2015;  
169 Wilczek et al., 2004; Zhang et al., 2018). Wet grinding is believed to better simulate the low-  
170 energy degradation of plastics in the environment than milling (Ravishankar et al., 2018). To the  
171 authors' knowledge, there are no commercially available sources of environmentally-relevant  
172 NPs other than monodisperse polystyrene spheres employed to calibrate laser light scattering  
173 and related techniques.

174 The objective of this study is therefore to develop a procedure that produces MPs and  
175 NPs from agricultural plastics (a mulch film composed of biodegradable polymer polybutyrate  
176 adipate-co-terephthalate (PBAT) and low-density PE [LDPE]), and to characterize the resultant  
177 materials in terms of size, size distribution and physicochemical properties. The methodology  
178 developed herein may also be useful to better understand the size reduction process that occur  
179 in nature, from mesoplastics to MPs (as would occur during plastics' tillage into the soil) and  
180 from MPs to NPs (as would simulate the low-impact shear events such as MP-soil collisions).

181

## 182 **2. EXPERIMENTAL**

### 183 ***2.1. Materials***



184 BioAgri, a black-colored biodegradable mulch film prepared from Mater-Bi® (Grade  
185 EF04P), a starch-copolyester blend containing PBAT as its major constituent, was kindly  
186 provided by BioBag Americas (Dunevin, FL, USA). The film referred to as “PBAT” in this  
187 paper, possesses an apparent density of  $22.81 \pm 0.411 \text{ g m}^{-2}$  thickness of  $29 \pm 1.2 \text{ }\mu\text{m}$ , peak load of  
188  $12.05 \pm 0.586 \text{ N}$  and an elongation of  $295.00 \pm 30.00 \%$  at maximum tensile stress, in the machine  
189 direction (Hayes et al., 2017). Other physicochemical properties are given in the cited reference.  
190 The original film was provided as a 1.22 m-wide roll and stored at  $20.6 \pm 2.1 \text{ }^\circ\text{C}$  and  $61.8 \pm 10.6\%$   
191 relative humidity. LDPE beads, with a nominal diameter of 3 mm and particle density of  $0.923$   
192  $\text{g cm}^{-3}$ , were purchased from Dow Chemicals (Midland, MI, USA). Chloroform (HPLC grade)  
193 was obtained from Fisher Scientific (Pittsburgh, PA, USA) and Acros Organics (Geel, Belgium),  
194 respectively. Deionized water was used throughout all experiments.

195

## 196 *2.2. Size reduction process to prepare MPs and NPs*

197 **Figure 1** outlines the overall procedure employed to prepare  $\mu\text{Ps}$  and  $\text{nPs}$  from PBAT  
198 and LDPE. Each of the process steps employed is described in detail below.

199

### 200 *2.2.1. Cryogenic treatment of PBAT*

201 PBAT films were cut with a paper cutter into strips with dimensions of  $\sim 120 \text{ mm}$   
202 (machine direction) x  $20 \text{ mm}$  (cross direction; **Figure S1**). The fragments ( $\sim 1.0 \text{ g}$ ) were  
203 presoaked in water (800 mL) for either 0, 5, or 10 min, recovered and transferred to a cryogenic  
204 container filled with liquid nitrogen (200 mL) and soaked for either 0, 5, or 10 min. The frozen  
205 PBAT film fragments (1.0 g) were transferred into an Osterizer type blender (Oster Accurate  
206 Blend 200, Boca Raton, FL, USA), and dry-comminuted for 10 s in order to break down the

207 solidified glass-like structure of the plastic. Water (400 mL) was added to the PBAT fragments  
208 to form a slurry, and then the blender was operated at a fixed duration (5 or 10 min) at an angular  
209 velocity of  $2 \times 10^{-3}$  or  $10 \times 10^{-3} \text{ min}^{-1}$ . After blending, the slurries were filtered under vacuum  
210 through a paper membrane filter (1  $\mu\text{m}$  mesh) using a Büchner funnel apparatus. Solid PBAT  
211 particles (depicted in **Figure S1**) were then air dried for 48 h to reduce moisture to  $< 1\%$ . A  
212 randomized experimental design was used to evaluate cryogenic processing conditions on  $d_p$   
213 achieved.

214

### 215 2.2.2. Microplastic ( $\mu\text{P}$ ) formation through milling and sieving

216 Cryogenic-treated PBAT fragments or untreated LDPE pellets ( $\sim 1.0 \text{ g}$ ) were fed to a  
217 rotary mill (Model 3383-L10 Wiley Mini Mill, fitted with screen, Arthur H. Thomas Co.,  
218 Philadelphia, PA, USA) by using sieve sizes of 20 mesh (840  $\mu\text{m}$ ) for the first pass and 60 mesh  
219 (250  $\mu\text{m}$ ) for the second pass through the mill. The residence time for milling was 20 min per  
220 pass. The particles recovered from milling ( $\sim 1.0 \text{ g}$  of PBAT or LDPE) were then fractionated  
221 via a cascade of four sieves (W.S. Tyler, Cleveland, OH, USA) with mesh sizes of #20 (840  $\mu\text{m}$ ),  
222 #60 (250  $\mu\text{m}$ ), #140 (106  $\mu\text{m}$ ), and #325 (45  $\mu\text{m}$ ). The latter three fractions are referred to herein  
223 as “ $\mu\text{Ps}$ ” (**Figure 1**). To enhance uniformity of the particle size distribution, the sieves were  
224 mounted on an Eppendorf thermomixer 5350 (Hamburg, Germany) and shaken for 30 min at  
225 300 rpm. The % recovery for each sieving fractions was determined gravimetrically for three  
226 replicate experiments.

227

### 228 2.2.3. Nanoplastic (NP) formation through high-performance wet grinding

229 An aqueous slurry (4.0 L) containing 1.00 wt % of MPs was prepared, which underwent  
230 stirring for 24 h to allow for a homogenous distribution. For this process, the 106  $\mu\text{m}$ -size MP-  
231 fraction was used rather than the to the smallest size MP fraction (45  $\mu\text{m}$ ) because the yield on  
232 the latter fraction was too small to provide sufficient amounts of material. After stirring, slurries  
233 were subjected to the wet-grinding process using a “supermass colloidier” (MKCA6-2, Masuko  
234 Sangyo, Tokyo, Japan) at a speed of 1500 rpm and 27 subsequent passes (collection of particles  
235 and reintroduction into the colloidier) to provide a uniform particle size reduction. The slurry  
236 recovered from wet-grinding was transferred to a 1000 mL beaker and magnetically stirred for  
237 4 h (300 rpm at 25°C). The resultant particles were dried at 40°C for 48 h and are referred to as  
238 “NPs” herein. Analyses of NPs were conducted using aliquots collected from the middle height  
239 position of the slurry so that NPs flocculating at the top and settling at the bottom of the slurry  
240 were not included. The final concentration of the slurry aliquots were 0.37 (wt)% and 0.28% for  
241 PAT and LDPE, respectively.

242

### 243 *2.3. Particle size analysis*

244 PBAT MPs formed via cryogenic treatment (**Figures 1 and S1**) were scanned by a  
245 flatbed-scanner (MX 490 by Canon, Tokyo, Japan) and the particle dimensions were analyzed  
246 by ImageJ software (Schneider et al., 2012). PBAT and LDPE MPs belonging to each of the  
247 four sieve fractions identified in **Figure 1** were analyzed via stereomicroscopy and images were  
248 analyzed using ImageJ software. Examples of images produced by ImageJ vs. the corresponding  
249 stereomicrographs are presented in **Figure 2**. The average MP diameter,  $d_p$ , was estimated using  
250 the Image J's “analyze particles” algorithm. The distribution of  $d_p$  derived from Image J analysis  
251 was fit by several different models using JMP<sup>®</sup> Pro 14.0 software (SAS Institute, Cary, NC,

252 USA). The corrected Akaike's and Bayesian information criteria (AIC and BIC, respectively)  
253 were used to compare the quality of model fits. All statistical evaluations employed a  
254 significance level of  $\alpha = 0.05$ . The size and size distribution of NPs was determined using  
255 dynamic light scattering (DLS) at 25°C. Detailed description of the procedures employed for  
256 size distribution of MPs and NPs is given in the **Supplementary Materials**.

#### 257 **2.4. Chemical and thermal analyses of the original plastics, MPs and NPs**

258 Chemical and thermal analyses were performed on the original polymeric materials, MPs  
259 (250  $\mu\text{m}$  sieve fraction; **Figure 1**), and NPs (produced after wet grinding) for both PBAT films  
260 and LDPE pellets. (For PBAT, samples were subjected to cryogenic treatment according to  
261 optimal conditions prior to milling and sieving). Analyses consisted of FTIR spectroscopy  
262 (chemical bonding properties), gel permeation chromatography (GPC; number- and weight-  
263 averaged molecular weight [ $M_n$  and  $M_w$ , respectively] and polydispersity index [ $PDI$ ;  $M_w/M_n$ ]),  
264 differential scanning calorimetry (DSC; properties), and thermogravimetric analysis (TGA;  
265 thermal stability). The instrumentation and detailed procedures are given in the **Supplementary**  
266 **Materials** and are nearly identical to those employed previously by the authors (Hayes et al.,  
267 2017).

268

### 269 **3. RESULTS AND DISCUSSION**

#### 270 **3.1. Effects of cryogenic treatment on the size reduction on PBAT mesoplastics**

271 For efficient size reduction of a biodegradable agricultural mulch film (PBAT),  
272 cryogenic treatment was applied to induce embrittlement, leading to size reduction (**Figure S1**).  
273 In the absence of cryogenic exposure, the PBAT film did not undergo size reduction upon  
274 mechanical milling (data not shown). A randomized design was used to evaluate the effect of

275 cryogenic treatment processing conditions (duration of pre-soaking in water and soaking in  
276 liquid nitrogen, and the blending speed, time and presence vs. absence of water) for the  
277 minimization of  $d_p$ . Factor levels were selected based on observations from preliminary blending  
278 experiments performed with PBAT films and accordingly the experimental matrix was selected  
279 (Table 1). A more detailed analysis of the  $d_p$  distribution is given in Table S1. Results showed  
280 that increased severity of processing conditions resulted in significant size reduction to  $d_p = 1$ -  
281 2 mm (Table 1, runs 4-6). Particularly, runs 4-6 shared the longest soaking time in liquid N<sub>2</sub> (10  
282 min), indicating that it is the most influential factor for size reduction. Similarly, a recent study  
283 focusing upon polystyrene  $\mu$ Ps found that the yield of  $\mu$ Ps increased with residence time during  
284 a pre-cooling step (Eitzen et al., 2019). Blending time and speed were also influential factors,  
285 but to a lesser extent than soaking time.

286 A further evaluation of the Table 1 data by prediction profiler statistical software  
287 confirms the trends discussed above, that liquid nitrogen soaking time was the major factor,  
288 followed by blending time and speed (Figure S2). Also, the statistical analysis demonstrated  
289 that no interaction within processing factors was observed, suggesting that increased levels for  
290 processing parameters will result in a more effective reduction of  $d_p$  (Figure S2). The inclusion  
291 of water resulted in a well-blended mixture, leading to a slight reduction of  $d_p$  (Figure S2). The  
292 software predicts that under optimal conditions, an average  $d_p$  value of 1.15 mm can be achieved  
293 (Figure S2), which is slightly lower than the minimal value of  $d_p$  achieved in Table 1, 1.43 mm.

294 A representative histogram for  $d_p$  of PBAT MPs produced by cryogenic treatment is  
295 shown in Figure 3, and histograms and particle counts for all runs of Table 1 are depicted in  
296 Figures S3 and S4, respectively. The smallest size fraction of Figure 3, 0-0.5 mm, serves as the  
297 largest fraction, and as the average  $d_p$  for fractions increases, the population size slowly

298 decreases. Several different size distribution models were evaluated for the quality of the fit to  
299 the data: Loglogistic, Frechet, Lognormal, and two-parameter Weibull. The latter distribution  
300 provided the best fit (followed by Lognormal), exhibited by the lowest AIC and BIC values  
301 obtained for the fit. The two-parameter Weibull model is described by:

$$302 \quad f(x, \alpha, \beta) = \begin{cases} \frac{\beta}{\alpha} \left(\frac{x}{\alpha}\right)^{\beta-1} \exp\left(-\left[\frac{x}{\alpha}\right]^{\beta}\right) & x \geq 0 \\ 0 & x < 0 \end{cases} \quad (1)$$

303 where  $\beta > 0$  is the shape parameter and  $\alpha > 0$  is the scale parameter of the distribution. The two-  
304 parameter Weibull model is a flexible distribution model that is applied to a broad range of  
305 applications such as bioproduct development (Varga et al., 2001), terrestrial sediments (Allen et  
306 al., 2015), quality engineering for material strength data distribution (Young et al., 2015), two-  
307 phase materials in metallurgy (Fang et al., 1993; Lynch and Rowland, 2005), aerosols (Dunbar  
308 and Hickey, 2000), seed sizes (Domoradzki and Korpál, 2005), and wind speed distribution in  
309 aerodynamics (Seguro and Lambert, 2000). Of relevance to this study, the two-parameter  
310 Weibull model has also been demonstrated to be the most effective size distribution model to  
311 describe soil particles (Bayat et al., 2015; Esmaelnejad et al., 2016).

312 The average  $d_p$  values obtained through the Weibull model fit,  $\alpha$  and  $\beta$  values, and  
313 information on the quality of the fit (AIC and BIC) are given in Table 1. Run 4, which provided  
314 the lowest  $d_p$ , also experienced the best fit of the two-parameter Weibull model to its size  
315 distribution data, evidenced by the minimization of AIC and BIC (Table 1).  $\beta$  values ( $\sim 1.0$ ) did  
316 not change appreciably with cryogenic conditions, and are reflective of a broad distribution with  
317 a maximum skewed toward the lower end of the distribution function (Table 1 and Figure 3).

318

### 319 3.2. Effects of mechanical milling on MP formation

320 The use of **mechanical** milling led to the formation of PBAT and LDPE **MPs** that were  
321 isolated at three different sieving fractions (**Figure 1**): 250  $\mu\text{m}$ , 106  $\mu\text{m}$ , and 45  $\mu\text{m}$  (plus larger  
322 particles at 840  $\mu\text{m}$ , which are also **MPs** according to definition (Alimi et al., 2018; Gigault et  
323 al., 2018; Hartmann et al., 2019) (**Figure 4**). More detailed information on the particle size  
324 distribution is given in **Table S2**. The mass recovery and  $d_p$  values for the two smallest sieve  
325 fractions, 106  $\mu\text{m}$  and 45  $\mu\text{m}$ , were nearly equal for both plastics with a mass recovery of 2 wt%  
326 and 1 wt%, respectively, and  $d_p$  values were nearly equal to the nominal sieve sizes (**Figure 4**).  
327 For 250  $\mu\text{m}$  fraction, the recovery was lower for PBAT (11%) than for LDPE (18%), and  $d_p$  was  
328 lower for the former plastic (and less than the nominal size). These results reflect that  
329 mechanically milled PBAT contains a larger amount of coarser, less geometrically uniform,  
330 particles than milled LDPE, likely a result of PBAT being a softer and less dense polymeric  
331 material. The same trend serves as the underlying cause of the larger variability in  $d_p$  for PBAT  
332 for the 840  $\mu\text{m}$  and 250  $\mu\text{m}$  sieve fractions (**Figure 4**). In summary, shear force via milling  
333 (supported by additional degradation **via** cryogenic treatment for PBAT) produced **MPs** at low-  
334 to-moderate yields.

335 Similar to PBAT  $\mu\text{P}$  particles obtained by cryogenic treatment, the size distribution of  $d_p$   
336 was best fit **by** a two-parameter Weibull model for all sieve fractions produced by milling  
337 (**Figures 5 and S5**). Parameters related to the fit of the Weibull model are given in **Table 2**,  
338 while particle count vs.  $d_p$  is depicted in **Figure S6**. The fit of the Weibull model improved as  
339 the sieve size of the fractions decreased, noted by a decrease of AIC and BIC (**Table 2**). Unlike  
340 the distribution obtained for cryogenic-treated **MPs**, which was skewed toward lower end of the  
341  $d_p$  distribution (i.e.,  $\beta \approx 1.0$ ; **Table 1**), for all sieve fractions, the distributions were slightly  
342 skewed in favor of higher  $d_p$  values ( $\beta > 8$ ; **Table 2**). The narrowest size distribution occurred

343 for the 45  $\mu\text{m}$  sieve fractions and for LDPE MP fractions compared to PBAT fractions (i.e.,  
344 highest  $\beta$  value), the latter trend reflecting coarser and less geometrically uniform particles for  
345 PBAT as discussed above. Therefore, the production of NPs was not detected, noting that the  
346 smallest size sieve fraction, 45  $\mu\text{m}$ , provided MP particles of size ( $d_p$ )  $\geq 36 \mu\text{m}$ . Moreover, it is  
347 unlikely that mechanical tilling of plastic mulch films will directly produce NPs.

### 348 3.3. Effects of wet-grinding on NP formation from $\mu\text{Ps}$

349 Wet grinding was applied to the 106  $\mu\text{m}$  MPs fraction of both plastics to produce NPs,  
350 with  $d_p$  measured by DLS. For both plastics, the particle size distributions possessed similar  
351 bimodal distribution, with the major and minor fractions (I and II, respectively, with I being  
352  $\sim 2.5$ -fold higher in intensity than II) possessing maxima at  $d_p$  values of  $\sim 500 \text{ nm}$  and  $\sim 60 \text{ nm}$ ,  
353 respectively (Figure 6). The size of fraction I is  $\sim 15$ -fold smaller than that of the initial 106  $\mu\text{m}$   
354 sieve fraction (Table 2 and Figure 5 a,c). Average  $d_p$  values for PBAT and LDPE NPs (i.e.,  
355 both fractions combined) were  $366.6 \pm 6.5 \text{ nm}$  and  $389.4 \pm 10.7 \text{ nm}$  (error bars reflect standard  
356 deviation), respectively, and spanned the range  $\sim 40$ - $1300 \text{ nm}$ , with the range of LDPE being  
357 slightly broader (Figure 6 and Table 3). These results suggest that degradation due to low shear  
358 may occur through two steps, one of which reduces size 15-fold and the other further reducing  
359 size by an additional factor of 10. For each fraction, lower  $d_p$  values were observed for LDPE,  
360 despite the original LDPE material possessing a higher  $d_p$  (Table 3 and Figure 5b). However,  
361 the aqueous solution of LDPE NPs produced by wet grinding contained a significant fraction of  
362 particles that flocculated on top that were not included in the sample analyzed by DLS. The  
363 flocculation is due to the density of LDPE being lower than that of water and the polymer's  
364 hydrophobicity. Another possible cause is the creeping of the NPs in the upward direction due  
365 to adhesion with the glass container walls, a phenomenon recently reported for polystyrene NPs



366 (Eitzen et al., 2019). The same study reported that adhesion was lessened when the polystyrene  
367 NPs were oxidized by ozone (Eitzen et al., 2019). Environmentally-weathered PE is known to  
368 undergo oxidation, forming polar functional groups on its surface such as hydroxyls and  
369 carboxylates (Hayes et al., 2017). It is likely that the flocculation of NPs formed from weathered  
370 LDPE would be lessened. In contrast, PBAT NPs were evenly dispersed throughout the slurry,  
371 even in the absence of stirring.

372 The size distribution model that fit the two NP fractions for each polymeric material was  
373 the two-parameter Weibull model (Figure 6). The smaller, ~60 nm –sized fractions (I) were  
374 narrower in the width of their size distributions than the larger size fraction (II), noted by the  
375 larger shape factor,  $\beta$  (Table 3), and both distributions were narrower than the original starting  
376 material, the 106 mm sieve fraction (Table 2). Future research is needed to better understand the  
377 relationship between wet grinding conditions and the resultant sizes and size distributions of the  
378 NP products.

379

### 380 3.4. Effect of size reduction on chemical and thermal properties of plastics

381 Chemical and thermal analyses of MPs and NPs were compared to the original plastic  
382 feedstock to determine if size reduction promoted any changes in properties.  $\mu$ P samples  
383 consisted of the 250 mm sieve fraction of dry milled plastics, while NPs were produced via wet  
384 grinding of the 106  $\mu$ m MPs sieve fraction.

385 The thermal stability of MPs and NPs was examined by analysis of TGA curves (Figures  
386 7 a,b) and differential thermograms (DTGs) (rate of heat loss vs. temperature; Figures 7c,d).  
387 For the PBAT-rich film, the first major heating stage was found at temperatures between 300°C  
388 and 318°C, representing the decomposition of starch, while the second, largest, stage (~400°C)

389 represents decomposition of PBAT (Hayes et al., 2017). The mass remaining at the maximum  
390 temperature, 600°C, reflects minor components such as binders and fillers, and perhaps gels  
391 (Hayes et al., 2017). No weight loss was observed for temperatures <200°C, suggesting the  
392 absence of water and volatiles. The formation of MPs led to a slight shifting of both major  
393 heating stages to lower temperatures (Figure 7a,c). Upon further size reduction to NPs, the  
394 heating stages for starch and PBAT are shifted more significantly to lower temperatures. For  
395 LDPE, while TGA curves were nearly identical for the original material and MPs, curve for  
396 NPs were slightly shifted to lower temperatures, to a much lesser extent than PBAT. (Figure 7  
397 b,d).

398 The loss of thermostability by starch, PBAT and LDPE is due to either a decrease of  
399 crystallinity or molecular weight. Crystallinity ( $X_c$ ) was measured via DSC via the enthalpy of  
400 melting (discussed in the Supplementary Materials). For both polymeric materials, cryogenic  
401 exposure followed by mechanical milling increased  $X_c$  nearly two-fold, and NPs and MP  
402 possessed similar values (Table 4). An increase of crystallinity was also observed during  
403 embrittlement caused by environmental weathering (Hayes et al., 2017). DSC analysis  
404 demonstrated that the melting and glass transition temperatures of PBAT and LDPE underwent  
405 slight changes (discussed in Supplementary Materials).

406 Therefore, the loss of thermostability is likely a result of depolymerization, a hypothesis  
407 supported by GPC analysis of PBAT. Depolymerization occurred slightly during the formation  
408 of MPs (i.e., cryogenic treatment followed by Wiley milling), noted by the 27.6% decrease of  
409  $M_w$ ; but, size reduction of MPs to NPs did not decrease  $M_w$  appreciably, 1.4% (Table 4). In  
410 contrast, the molecular weight distribution was narrower (i.e., PDI lower) and  $M_n$  slightly higher  
411 for MPs compared to the original polymeric film, and for NPs compared to MPs, suggesting the

412 lower-molecular weight polymers were removed during milling and wet grinding (**Table 4**).  
413 These trends may reflect the selective degradation of local regions that are weaker in strength  
414 (e.g., amorphous morphological regions), where lower molecular weight polymers would be  
415 expected to reside. In contrast, smaller particles recovered from wet grinding of plastics typically  
416 undergo a slight decrease of  $M_n$  and  $M_w$  and a minor increase of PDI (Ravishankar et al., 2018).  
417 Herein, NP samples were taken from the middle layer of the slurry, such that smaller particles,  
418 which flocculated near the top layer, were less likely to have been contained in the sample.

419 TGA also provides the relative proportion of components, such as PBAT and starch. Size  
420 reduction to MPs decrease the starch content from 16.8% to 13.0%, and further size reduction  
421 to NPs further reduced the starch content to 8.3% (**Figure 7a,c**). In contrast, the PBAT content  
422 of the original film and MPs were nearly identical (71.6 and 70.6%, respectively) and NPs  
423 possessed a 12% lower PBAT content (62.2%; **Figure 7a,c**). These results demonstrate that the  
424 size-reduced starch was readily leached away from MPs and NPs, while the slight loss of PBAT  
425 upon formation of NPs is due to both leaching away of lower-molecular weight polymers and  
426 the formation of a gel-like material, noted by the increase of mass remaining at 600°C (**Figure**  
427 **7a,c**). FTIR analysis also reflected the reduction of starch content upon size reduction, the  
428 occurrence of hydrolysis and the absence of oxidation-reduction reactions (e.g., the absence of  
429 cross-link formation or new functional surface groups; discussed in **Supplementary Materials**).

430

#### 431 4. CONCLUSIONS

432 In this study, a simple and effective size reduction process was developed to prepare MPs and  
433 NPs from prominent agricultural plastics, PBAT-rich biodegradable mulch films and LDPE, that  
434 are more likely to represent MPs and NPs occurring in agricultural soils, in contrast to

435 monodisperse polystyrene beads and other commonly employed model materials in fundamental  
436 studies. The protocol consisted of cryogenic treatment (to mimic the embrittlement caused by  
437 environmental weathering), followed by mechanical milling (to prepare MPs of nominal sizes  
438 45  $\mu\text{m}$ , 106  $\mu\text{m}$ , 250  $\mu\text{m}$  and 840  $\mu\text{m}$ , mimicking the impact of cutting and high-impact  
439 mechanical degradation and that occur during tillage of plastics into soil). The 106  $\mu\text{m}$  MP  
440 fraction was subjected to wet grinding, a process that mimics low-impact shear as would occur  
441 between MPs and soil particulates or water (Ravishankar et al., 2018), to produce NPs. The  
442 latter's size distribution was bimodal, with the average size of the two populations being 15- and  
443 150-fold smaller than the original 106  $\mu\text{m}$  MP fraction. The size distribution of MPs and the two  
444 NP subpopulations was described effectively by the two-parameter Weibull function, and the  
445 former was quite broad. Degradation occurred at locally weaker regions possessing lower  
446 crystallinity and average molecular weight, and was assisted by the leaching away of polar and  
447 lower molecular weight components, such as starch from the PBAT film. The procedure  
448 described herein can be applied to several plastic materials, including residual plastic film  
449 fragments or debris, to form representative terrestrial MP and NPs materials for future  
450 environmental studies, such as ecotoxicity screening and the transport and fate of MPs and NPs  
451 in soil ecosystems. The methodology described herein can be employed to investigate the  
452 formation of MPs and NPs, such as the kinetics and time course of size reduction, the effect of  
453 environmental parameters such as temperature, salinity or the presence of soil particulates.

454

## 455 5. ACKNOWLEDGMENTS

456 Financial support for this research was provided by the seed grant program of the Institute  
457 for a Secure and Sustainable Environment (ISSE) of the University of Tennessee (UT), the

458 USDA Specialty Crops Research Initiative, Coordinated Agricultural Project (Award 2014-  
459 51181-22382), and the UT Institute of Agriculture. Ms. Galina Melnichenko and Ms. Marife  
460 Anunciado assisted with the collection of GPC data. Dr. David Harper provided technical  
461 assistance. We are grateful to BioBag Americas, Inc. (Dunevin, FL, USA) for their kind donation  
462 of BioAgri biodegradable mulch film, serving as the source of PBAT.

463

## 464 **6. APPENDIX A. SUPPLEMENTARY MATERIALS**

465 Supplementary data and information associated with this article can be found in the online  
466 version.

467

## 468 **7. FIGURE CAPTIONS**

469 **Figure 1.** Flow diagram for processing of micro- and nanoplastics (MPs and NPs, respectively)





470

471 **Figure 2.** Stereomicrographs of MPs (250  $\mu\text{m}$  fraction resulting from milling followed by  
472 sieving; cf. **Figure 1**): (a) PBAT and (c) LDPE, and (b) and (d) the corresponding images  
473 produced by Image J software using for the watershed function. Prior to milling, PBAT film  
474 samples underwent cryogenic treatment according to the conditions of Run 4 of **Table 1**.

475

476 **Figure 3.** Particle size distribution of PBAT MPs resulting from the cryogenic treatment  
477 represented by Run 4 of **Table 1**. The red curve represents the fit of the two-parameter Weibull  
478 model (*Eq. 1*) to the data.

479

480 **Figure 4.** Average particle size ( $d_p$ ) and % recovery of mass for **MPs** of PBAT ( and ,  
481 **respectively**) and LDPE ( and , **respectively**) obtained via dry milling (840  $\mu\text{m}$  and 250  $\mu\text{m}$   
482 sieves for the first and second pass) of 1g of feed, followed by sieving. Sieve sizes are indicated  
483 by solid black bars in the figures.  $d_p$  was determined by Image J analysis of stereomicrographs  
484 to fit the histogram for size distribution. Errors for  $d_p$  represent one standard deviation. LDPE  
485 particles were directly fed to the mill, while for PBAT, the feed was treated by cryogenic  
486 treatment according to optimal conditions (Run 4 of **Table I**). The inset shows  $d_p$  and % recovery  
487 for the largest, 841  $\mu\text{m}$ , sieve fraction.

488  
489 **Figure 5.** Particle size distributions of **(a,b)** PBAT and **(c,d)** LDPE for the **(a,c)** 45  $\mu\text{m}$  and **(b,d)**  
490 106  $\mu\text{m}$  nominal **MP** sieve fractions (after mechanical milling), with superimposed two-  
491 parameter Weibull model (**Eq. 1**).

492  
493 **Figure 6.** Histograms of particle size ( $d_p$ ) for **a** PBAT and **b** LDPE **NPs**, formed from the wet-  
494 grinding treatment of the 106  $\mu\text{m}$ -**MP** sieve fraction. **Error bars** represent  $\pm$ one standard  
495 deviation of the dataset. Curves represent two-parameter Weibull model fits to **size distribution**  
496 fractions **I** and **II**, as listed in **Table 3**.

497  
498 **Figure 7. a,b** TGA and **c,d** DTG curves before processing initial polymer, after dry-milling  
499 (**MPs**) and wet grinding (**NPs**) of **(a,c)** PBAT and **(b,d)** LDPE. **MPs** consist of the 250  $\mu\text{m}$  sieve  
500 fraction of dry milled plastics (cryogenic treatment applied to PBAT according to the optimal  
501 conditions: Run 4 of **Table I**); **NPs** were produced via wet grinding of the 106  $\mu\text{m}$  sieve fraction  
502  $\mu\text{Ps}$  after dry milling.

503

504 **REFERENCES**

- 505 Alimi, O. S., Farner Budarz, J., Hernandez, L. M., Tufenkji, N., 2018. Microplastics and  
506 nanoplastics in aquatic environments: aggregation, deposition, and enhanced  
507 contaminant transport. *Environ. Sci. Technol.* 52, 1704-1724.
- 508 Allen, P. A., Michael, N. A., D'Arcy, M., Roda-Boluda, D. C., Whittaker, A. C., Duller, R. A.,  
509 Armitage, J. J., 2015. Fractionation of grain size in terrestrial sediment routing systems.  
510 *Basin Res.* 29, 180-202.
- 511 Bayat, H., Rastgo, M., Mansouri Zadeh, M., Vereecken, H., 2015. Particle size distribution  
512 models, their characteristics and fitting capability. *J. Hydrol.* 529, 872-889.
- 513 Bläsing, M., Amelung, W., 2018. Plastics in soil: Analytical methods and possible sources. *Sci.*  
514 *Total Environ.* 612, 422-435.
- 515 Bouwmeester, H., Hollman, P. C. H., Peters, R. J. B., 2015. Potential health impact of  
516 environmentally released micro- and nanoplastics in the human food production chain:  
517 experiences from nanotoxicology. *Environ. Sci. Technol.* 49, 8932-8947.
- 518 Corradini, F., Bartholomeus, H., Huerta Lwanga, E., Gertsen, H., Geissen, V., 2019. Predicting  
519 soil microplastic concentration using vis-NIR spectroscopy. *Sci. Total Environ.* 650,  
520 922-932.
- 521 de Souza Machado, A. A., Kloas, W., Zarfl, C., Hempel, S., Rillig, M. C., 2017. Microplastics  
522 as an emerging threat to terrestrial ecosystems. *Global Change Biol.* 24, 1405-1416.
- 523 Domoradzki, M., Korpala, W., 2005. Seed size dependent germination of selected vegetables.  
524 *Acta Agrophys.* 5, 607-612.

525 Dümichen, E., Barthel, A.-K., Braun, U., Bannick, C. G., Brand, K., Jekel, M., Senz, R., 2015.  
526 Analysis of polyethylene microplastics in environmental samples, using a thermal  
527 decomposition method. *Water Res.* 85, 451-457.

528 Dunbar, C. A., Hickey, A. J., 2000. Evaluation of probability density functions to approximate  
529 particle size distributions of representative pharmaceutical aerosols. *J. Aerosol Sci.* 31,  
530 813-831.

531 Eckert, E. M., Di Cesare, A., Kettner, M. T., Arias-Andres, M., Fontaneto, D., Grossart, H.-P.,  
532 Corno, G., 2018. Microplastics increase impact of treated wastewater on freshwater  
533 microbial community. *Environ. Pollut.* 234, 495-502.

534 Efsa Panel on Contaminants in the Food Chain, 2016. Presence of microplastics and nanoplastics  
535 in food, with particular focus on seafood. *EFSA J.* 14, 4501.

536 Eitzen, L., Paul, S., Braun, U., Altmann, K., Jekel, M., Ruhl, A. S., 2019. The challenge in  
537 preparing particle suspensions for aquatic microplastic research. *Environ. Res.* 168, 490-  
538 495.

539 Elkharraz, K., Dashevsky, A., Bodmeier, R., 2003. Microparticles prepared by grinding of  
540 polymeric films. 20, 661-673.

541 Esmaelnejad, L., Siavashi, F., Seyedmohammadi, J., Shabanpour, M., 2016. The best  
542 mathematical models describing particle size distribution of soils. *Model. Earth Syst.*  
543 *Environ.* 2, 1-11.

544 Fang, Z., Patterson, B. R., Turner, M. E., 1993. Modeling particle size distributions by the  
545 Weibull distribution function. *Mater. Charact.* 31, 177-182.



546 Gigault, J., Halle, A. t., Baudrimont, M., Pascal, P.-Y., Gauffre, F., Phi, T.-L., El Hadri, H.,  
547 Grassl, B., Reynaud, S., 2018. Current opinion: What is a nanoplastic? Environ. Pollut.  
548 235, 1030-1034.

549 Goedecke, C., Mülow-Stollin, U., Hering, S., Richter, J., Piechotta, C., Paul, A., Braun, U., 2017.  
550 A First Pilot Study on the Sorption of Environmental Pollutants on Various Microplastic  
551 Materials. J. Environ. Anal. Chem. 4, 191.

552 Guo, X., Pang, J., Chen, S., Jia, H., 2018. Sorption properties of tylosin on four different  
553 microplastics. Chemosphere. 209, 240-245.

554 Hartmann, N. B., et al., 2019. Are we speaking the same language? Recommendations for a  
555 definition and categorization framework for plastic debris. Environ. Sci. Technol. 53,  
556 1039-1047.

557 Hayes, D. G., et al., Biodegradable plastic mulch films for sustainable specialty crop production.  
558 In: T. J. Gutierrez, (Ed.), Polymers for Agri-Food Applications. Springer Nature, Berlin,  
559 2019, pp. in press.

560 Hayes, D. G., Wadsworth, L. C., Sintim, H. Y., Flury, M., English, M., Schaeffer, S., Saxton, A.  
561 M., 2017. Effect of diverse weathering conditions on the physicochemical properties of  
562 biodegradable plastic mulches. Polym. Testing. 62, 454-467.

563 Horton, A. A., Walton, A., Spurgeon, D. J., Lahive, E., Svendsen, C., 2017. Microplastics in  
564 freshwater and terrestrial environments: Evaluating the current understanding to identify  
565 the knowledge gaps and future research priorities. Sci. Total Environ. 586, 127-141.

566 Huerta Lwanga, E., Gertsen, H., Gooren, H., Peters, P., Salánki, T., van der Ploeg, M., Besseling,  
567 E., Koelmans, A. A., Geissen, V., 2017. Incorporation of microplastics from litter into  
568 burrows of *Lumbricus terrestris*. Environ. Pollut. 220, 523-531.

569 Hussain, I., Hamid, H., *Plastics in Agriculture*. In: A. L. Andrady, (Ed.), *Plastics and the*  
570 *Environment*. John Wiley and Sons, New York, 2003, pp. 185-209.

571 Jambeck, J. R., Geyer, R., Wilcox, C., Siegler, T. R., Perryman, M., Andrady, A., Narayan, R.,  
572 Law, K. L., 2015. Plastic waste inputs from land into the ocean. *Science*. 347, 768.

573 Jonna, S., Lyons, J., 2005. Processing and properties of cryogenically milled post-consumer  
574 mixed plastic waste. *Polym. Testing*. 24, 428-434.

575 Kasirajan, S., Ngouajio, M., 2012. Polyethylene and biodegradable mulches for agricultural  
576 applications: a review. *Agron. Sustain. Dev.* 32, 501-529.

577 Koelmans, A. A., Besseling, E., Wegner, A., Foekema, E. M., 2013. Plastic as a carrier of POPs  
578 to aquatic organisms: a model analysis. *Environ Sci Technol*. 47.

579 Kühn, S., van Oyen, A., Booth, A. M., Meijboom, A., van Franeker, J. A., 2018. Marine  
580 microplastic: Preparation of relevant test materials for laboratory assessment of  
581 ecosystem impacts. *Chemosphere*. 213, 103-113.

582 Lu, L., Wan, Z., Luo, T., Fu, Z., Jin, Y., 2018. Polystyrene microplastics induce gut microbiota  
583 dysbiosis and hepatic lipid metabolism disorder in mice. *Sci. Total; Environ*. 631-632,  
584 449-458.

585 Lynch, A. J., Rowland, C. A., 2005. *The History of Grinding*. Society for Mining, Metallurgy,  
586 and Exploration, Inc., Littleton, CO, USA.

587 Mattsson, K., Hansson, L. A., Cedervall, T., 2015. Nano-plastics in the aquatic environment.  
588 *Environ. Sci.: Processes Impacts*. 17, 1712-1721.

589 McCormick, A., Hoellein, T. J., Mason, S. A., Schlupe, J., Kelly, J. J., 2014. Microplastic is an  
590 abundant and distinct microbial habitat in an urban river. *Environ. Sci. Technol*. 48,  
591 11863-11871.

592 Miles, C., DeVetter, L., Ghimire, S., Hayes, D., G., 2017. Suitability of biodegradable plastic  
593 mulches for organic and sustainable agricultural production systems. *HortSci.* 52, 10-15.

594 Ng, E.-L., Huerta Lwanga, E., Eldridge, S. M., Johnston, P., Hu, H.-W., Geissen, V., Chen, D.,  
595 2018. An overview of microplastic and nanoplastic pollution in agroecosystems. *Sci.*  
596 *Total Environ.* 627, 1377-1388.

597 Nizzetto, L., Futter, M., Langaas, S., 2016. Are agricultural soils dumps for microplastics of  
598 urban origin? *Environ. Sci. Technol.* 50, 10777-10779.

599 Oberbeckmann, S., Kreikemeyer, B., Labrenz, M., 2018. Environmental Factors Support the  
600 Formation of Specific Bacterial Assemblages on Microplastics. *Front. Microbiol.* 8, 2709.

601 Poulouse, A. M., Piccarolo, S., Carbone, D., Al-Zahrani, S. M., 2016. Influence of plasticizers  
602 and cryogenic grinding on the high-cooling-rate solidification behavior of PBT/PET  
603 blends. *J. Appl. Polym. Sci.* 133, 43083.

604 Ravishankar, K., Ramesh, P. S., Sadhasivam, B., Raghavachari, D., 2018. Wear-induced  
605 mechanical degradation of plastics by low-energy wet-grinding. *Polym. Degr. Stab.* 158,  
606 212-219.

607 Robotti, M., Dosta, S., Cano, I. G., Concustell, A., Cinca, N., Guilemany, J. M., 2016. Attrition  
608 and cryogenic milling powder production for low pressure cold gas spray and composite  
609 coatings characterization. *Adv. Powder Technol.* 27, 1257-1264.

610 Saba, N., Tahir, P. M., Abdan, K., Ibrahim, N. A., 2015. Preparation and characterization of fire  
611 retardant nanofiller from oil palm empty fruit bunch fibers. *BioResources.* 10, 4530-4543.

612 Scarascia-Mugnozza, G., Sica, C., Russo, G., 2011. Plastic materials in European agriculture:  
613 actual use and perspectives. *J. Agric. Eng.* 42, 15-28.

614 Scheurer, M., Bigalke, M., 2018. Microplastics in Swiss floodplain soils. Environ. Sci. Technol.  
615 52, 3591-3598.

616 Schmidt, J., Plata, M., Tröger, S., Peukert, W., 2012. Production of polymer particles below 5µm  
617 by wet grinding. Powder Technol. 228, 84-90.

618 Schmidt, J., Romeis, S., Peukert, W., 2017. Production of PBT/PC particle systems by wet  
619 grinding. AIP Conf. Proc. 1914, 050003.

620 Schneider, C. A., Rasband, W. S., Eliceiri, K. W., 2012. NIH Image to ImageJ: 25 years of image  
621 analysis. Nature Meth. 9, 671.

622 Schwabl, P., Liebmann, B., Köppel, S., Königshofer, P., Bucsics, T., Trauner, M., Reiberger, T.,  
623 Assessment of microplastics concentrations in human stool: preliminary results (United  
624 European Gastroenterology Conference, Vienna, Austria, 20-24 October 2018). Vol. 2019,  
625 2018.

626 Seguro, J. V., Lambert, T. W., 2000. Modern estimation of the parameters of the Weibull wind  
627 speed distribution for wind energy analysis. J. Wind Eng. Ind. Aerodyn. 85, 75-84.

628 Steinmetz, Z., Wollmann, C., Schaefer, M., Buchmann, C., David, J., Tröger, J., Muñoz, K.,  
629 Frör, O., Schaumann, G. E., 2016. Plastic mulching in agriculture. Trading short-term  
630 agronomic benefits for long-term soil degradation? Sci. Total Environ. 550, 690-705.

631 Varga, E. G., Titchener-Hooker, N. J., Dunnill, P., 2001. Prediction of the pilot-scale recovery  
632 of a recombinant yeast enzyme using integrated models. Biotechnol. Bioeng. 74, 96-107.

633 von Moos, N., Burkhardt-Holm, P., Kohler, A., 2012. Uptake and effects of microplastics on  
634 cells and tissue of the blue mussel *Mytilus edulis* L. after an experimental exposure.  
635 Environ. Sci. Technol. 46.

636 Watano, S., Matsuo, M., Nakamura, H., Miyazaki, T., 2015. Improvement of dissolution rate of  
637 poorly water-soluble drug by wet grinding with bio-compatible phospholipid polymer.  
638 Chem. Eng. Sci. 125, 25-31.

639 Wilczek, M., Bertling, J., Hintemann, D., 2004. Optimised technologies for cryogenic grinding.  
640 Int. J. Mineral Proc. 74, S425-S434.

641 Wright, S. L., Kelly, F. J., 2017. Plastic and human health: a micro issue? Environ. Sci. Technol.  
642 51, 6634-6647.

643 Xu, B., Liu, F., Brookes, P. C., Xu, J., 2018. Microplastics play a minor role in tetracycline  
644 sorption in the presence of dissolved organic matter. Environ. Pollut. 240, 87-94.

645 Young, T. M., León, R. V., Chen, C.-H., Chen, W., Guess, F. M., Edwards, D. J., 2015. Robustly  
646 estimating lower percentiles when observations are costly. Quality Eng. 27, 361-373.

647 Zhang, Y., Fei, S., Yu, M., Guo, Y., He, H., Zhang, Y., Yin, T., Xu, H., Tang, X., 2018. Injectable  
648 sustained release PLA microparticles prepared by solvent evaporation-media milling  
649 technology. Drug Dev. Ind. Pharm. 44, 1591-1597.

650 Zhu, D., Chen, Q.-L., An, X.-L., Yang, X.-R., Christie, P., Ke, X., Wu, L.-H., Zhu, Y.-G., 2018.  
651 Exposure of soil collembolans to microplastics perturbs their gut microbiota and alters  
652 their isotopic composition. Soil Biol. Biochem. 116, 302-310.

653 Zuo, L.-Z., Li, H.-X., Lin, L., Sun, Y.-X., Diao, Z.-H., Liu, S., Zhang, Z.-Y., Xu, X.-R., 2019.  
654 Sorption and desorption of phenanthrene on biodegradable poly(butylene adipate co-  
655 terephthalate) microplastics. Chemosphere. 215, 25-32.

656

657